Available online at www.sciencedirect.com
SCIENCE DIRECT®
ELSEVIER
International Journal of Solids and Structures 43 (2006) 2479–2496
INTERNATIONAL JOURNAL OF SOLIDS and STRUCTURES
www.elsevier.com/locate/ijsolstr

Low-velocity impact response of sandwich beams with functionally graded core

N.A. Apetre [a], B.V. Sankar [a,*], D.R. Ambur [b]

[a] *Department of Mechanical and Aerospace Engineering, University of Florida, Gainesville, FL 32611-6250, United States*
[b] *NASA Glenn Research Center, 21000 Brookpark Road, Cleveland, OH 44135, United States*

Received 10 January 2005; received in revised form 31 May 2005
Available online 20 July 2005

Abstract

The problem of low-speed impact of a one-dimensional sandwich panel by a rigid cylindrical projectile is considered. The core of the sandwich panel is functionally graded such that the density, and hence its stiffness, vary through the thickness. The problem is a combination of static contact problem and dynamic response of the sandwich panel obtained via a simple nonlinear spring-mass model (quasi-static approximation). The variation of core Young's modulus is represented by a polynomial in the thickness coordinate, but the Poisson's ratio is kept constant. The two-dimensional elasticity equations for the plane sandwich structure are solved using a combination of Fourier series and Galerkin method. The contact problem is solved using the assumed contact stress distribution method. For the impact problem we used a simple dynamic model based on quasi-static behavior of the panel—the sandwich beam was modeled as a combination of two springs, a linear spring to account for the global deflection and a nonlinear spring to represent the local indentation effects. Results indicate that the contact stiffness of the beam with graded core increases causing the contact stresses and other stress components in the vicinity of contact to increase. However, the values of maximum strains corresponding to the maximum impact load are reduced considerably due to grading of the core properties. For a better comparison, the thickness of the functionally graded cores was chosen such that the flexural stiffness was equal to that of a beam with homogeneous core. The results indicate that functionally graded cores can be used effectively to mitigate or completely prevent impact damage in sandwich composites.

Keywords: Contact problem; Functionally graded cores; Functionally graded materials; Impact damage; Low-velocity impact; Sandwich panels

* Corresponding author. Tel.: +1 352 392 6749; fax: +1 352 392 7303.
E-mail address: sankar@ufl.edu (B.V. Sankar).

0020-7683/$ - see front matter © 2005 Elsevier Ltd. All rights reserved.
doi:10.1016/j.ijsolstr.2005.06.003

0. Introduction

Weight savings offered by sandwich constructions for structures that require high bending stiffness and buckling loads are significant. However, sandwich constructions have not been fully exploited in structural applications due to damage tolerance concerns. Debonding at or near the core/face sheet interface is a major problem in sandwich construction. The stiffness discontinuity at the face sheet/core interface results in a large increase in interfacial shear stresses. While the core material itself may withstand very high shear stresses, the bond (or adhesive layer) at the interface is usually weaker. It has been observed that stronger interface causes tearing of the core below the interface (Avery and Sankar, 2000). Although sandwich structures offer advantages over other types of structures, it is important to develop new types of materials in order to obtain the absolute minimum weight for given conditions such as structural geometry and loadings. These new sandwiches should be compared with other sandwich construction as well as with alternative structures in order to select the best configuration. One of the new alternatives is a sandwich structure with functionally graded core. In this paper, we explore the possibility of reducing the interfacial shear stresses and also the maximum strains in the core by grading the core properties in the thickness direction. This will be accomplished by minimizing the jump in the stiffness across the interface.

Functionally graded materials (FGMs) possess properties that vary gradually with location within the material such a way as to optimize some function of the overall FGM. FGMs differ from composites wherein the volume fraction of the inclusion is uniform throughout the composite. The closest analogies of FGMs are laminated composites, but they possess distinct interfaces across which properties change abruptly.

Nature provides many examples of functionally graded materials. They can be found in bones, plant stems (e.g., bamboo; Amada and Untao, 2001; Amada et al., 1997) and soils. Manufacturing methods include: high-speed centrifugal casting method (Fukui et al., 1997; Fukui, 1991); ultraviolet radiations (Lambros et al., 1999); electrophoretic deposition (Sarkar et al., 1997); dispersing microballoons (with linear graded volume fraction) in epoxy (El-Hadek and Tippur, 2003); high temperature infiltration (Suresh, 2001); chemical vapor deposition, powder metallurgy, plasma sprays, and self-propagating combustion synthesis (Koizumi, 1997).

Although fabrication technology of FGMs is in its infancy, they have great potential in many applications ranging from dental implants (Watari et al., 1997) to thermal coatings and thermal protection systems (Koizumi, 1997). Suresh and Mortensen (1998) provide an excellent introduction to properties, processing and characterization of FGMs.

As the use of FGMs increases in aerospace, automotive and biomedical applications, new methodologies have to be developed to characterize them, and to design and analyze structural components made with these materials. The methods should be such that they can be incorporated into available methods with minimal modifications, if any. One problem is that of response of structures made of FGMs to thermo-mechanical loads. Although FGMs are highly heterogeneous, it will be useful to idealize them as continua with properties that change smoothly with respect to spatial coordinates. This will enable closed-form solutions for some fundamental solid mechanics problems, and will aid the development of finite element models for structures made of FGMs.

Aboudi et al. (1994a,b, 1999) developed a higher order micro-mechanical theory for FGMs (HOTFGM) that explicitly couples local and global effects. They used higher-order representation of the temperature and displacement fields in order to capture the local effects created by the thermo-mechanical field gradients, the microstructure of the composite and the finite dimensions in the functionally graded directions. Later the theory was extended to free-edge problems by Aboudi and Pindera (1995) and to inelastic materials (Aboudi et al., 1995). Pindera and Dunn (1995) evaluated the higher order theory by performing a detailed finite element analysis of the FGM. They found that the HOTFGM results agreed well with the FE results. Marrey and Sankar (1993) studied the effects of stress gradients in textile composites consisting of unit cells large compared to the thickness of the composite. Their method resulted in direct computation

of plate stiffness coefficients from the micro-mechanical models rather than from the homogeneous elastic constants of the composite and plate thickness.

When using analytical methods to solve problems involving FGMs, a functional form for the variation of thermo-elastic constants has to be assumed. For example, Aboudi et al. (1994a,b, 1999) assumed a simple polynomial approximation for the elastic constants. Another useful approximation is the exponential variation, where the elastic constants vary according to formulas of the type $c_{ij} = c_{ij}^0 e^{\lambda z}$. Many researchers have found this functional form of property variation to be convenient in solving elasticity problems. For example, Delale and Erdogan (1983) derived the crack-tip stress fields for an inhomogeneous cracked body with constant Poisson ratio and a shear modulus variation given by $\mu = \mu_0 e^{(\alpha x+\beta y)}$.

Abid Mian and Spencer (1998) present an exact solution for three-dimensional elasticity equations for isotropic linearly elastic, inhomogeneous materials generalized from solutions for stretching and bending of symmetrically inhomogeneous plates. It is shown that the exact three-dimensional solutions are generated by two-dimensional solutions of the thin-plate equations for a homogeneous plate. Reddy and Cheng (2001) and Reddy (2000) use an asymptotic method to determine three-dimensional thermo-mechanical deformations of FG rectangular plates. Rooney and Ferrari (1999) developed solutions for tension, bending and flexure of an isotropic prismatic bar with elastic moduli varying across the cross-section. Vel and Batra (2002, 2003, 2004) present an exact solution for simply supported functionally graded rectangular thick or thin plates. The material has a power-law through-the-thickness variation of the volume fractions of the constituents and they employ a power series method to solve the equations. Woo and Meguid (2000) provide an analytical solution for the coupled large deflection of plates and shallow shells made of FGMs under transverse mechanical load and temperature field. The material properties of the shell are assumed to vary continuously through the thickness of the shell, according to a power law of volume fraction of the constituents. The equations obtained using von Karman theory for large transverse deflection, are solved by Fourier series method.

One of the important problems in sandwich structures is damage due to low velocity impact. The interfacial shear stresses due to the contact forces can be large enough to cause debonding of the face sheet from the core. One way of reducing the shear stresses is to use functionally graded core so that the abrupt change in stiffness between the face sheet and the core can be eliminated or minimized. The stresses that arise due to low-velocity impact can be easily understood by analyzing the static contact between the impactor and the structure (Sun and Sankar, 1985).

In a series of papers Sankar and his coworkers (Sankar and Tzeng, 2002; Sankar, 2001; Venkataraman and Sankar, 2001; Apetre et al., 2002) reported analytical methods for the thermo-mechanical and contact analysis of FG beams and also sandwich beams with FG cores. In these studies the thermo-mechanical properties of the FGM were assumed to vary through the thickness in an exponential fashion, e.g., $E(z) = E_0 e^{\lambda z}$. The material was assumed to be isotropic and the Poisson's ratio was assumed to be constant. The exponential variation of elastic stiffness coefficients allows exact elasticity solution via Fourier transform methods. Later, Apetre et al. (2003) and Zhu and Sankar (2004) used Galerkin method to analyze cores with polynomial variation of mechanical properties. In the present paper, we address the low-speed impact problem of a sandwich structure with FG core. It is demonstrated that maximum strains in the core for a given impact energy can be reduced significantly. Thus, there is a potential for using FGM cores in sandwich structures to minimize impact damage.

1. Solution via Fourier–Galerkin method for polynomial variation of core properties

Zhu and Sankar (2004) derived an analytical model for a FG beam with Young's modulus expressed as a polynomial in thickness coordinate using a combined Fourier series–Galerkin method. In the present work, the model is applied to a sandwich beam with FG core.

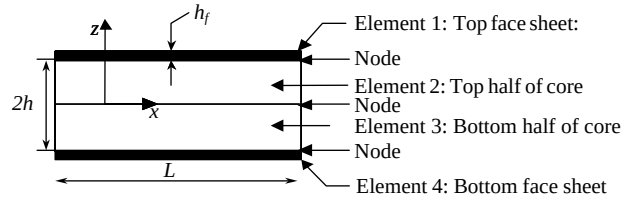

Fig. 1. Sandwich beam with functionally graded core divided into four elements.

The dimensions of the sandwich beam are shown in Fig. 1. The length of the beam is L, the core thickness is h and the face sheet thicknesses are h_f. The beam is divided into four parts or elements: the top face sheet, top half of the core, bottom half of the core and the bottom face sheet.

Each element has its own coordinate systems. The coordinate systems for each element are chosen at the interface, because it will be convenient to enforce displacement compatibility and continuity of tractions between elements at the interface nodes. The face sheets are assumed to be homogeneous and isotropic. The core is orthotropic at every point. The elasticity equations are formulated separately for each element, and compatibility of displacements and continuity of tractions are enforced at each interface (node) to obtain the displacement and stress field in the sandwich beam (Fig. 2). This procedure is analogous to assembling element stiffness matrices to obtain global stiffness matrix in finite element analysis.

Let us assume that the top face sheet is subjected to normal tractions such that,

$$\sigma_{zz}(x,0) = p_a \sin(\xi x), \tag{1}$$

where

$$\xi = \frac{n\pi}{L}, \quad n = 1,3,5,\ldots, \tag{2}$$

and p_a is known. Since n is assumed to be odd, the loading is symmetric about the center of the beam. The loading given by Eq. (1) is of practical significance because any arbitrary loading can be expressed as a Fourier series involving terms of the same type.

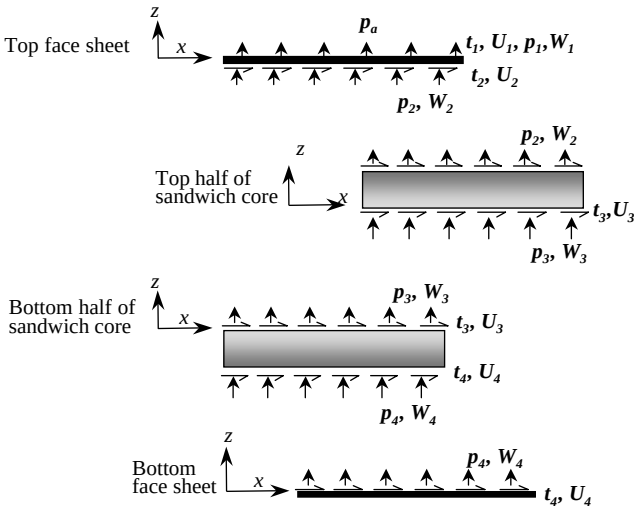

Fig. 2. Traction forces and displacements at the interfaces of each element in the FGM sandwich beam.

In this paper, we will provide a brief description of the procedures in order to obtain the stiffness matrix of top half of the core. The derivation of stiffness matrices of other elements follows the same procedures.

The differential equations of equilibrium for the top half of the core are

$$\frac{\partial \sigma_{xx}}{\partial x}+\frac{\partial \tau_{xz}}{\partial z}=0, \qquad \frac{\partial \tau_{xz}}{\partial x}+\frac{\partial \sigma_{zz}}{\partial z}=0. \tag{3}$$

If the core material is orthotropic at every point and the principal material directions coincide with the x- and z-axes, the constitutive relations are

$$\begin{Bmatrix} \sigma_{xx} \\ \sigma_{xx} \\ \tau_{xz} \end{Bmatrix} = \begin{bmatrix} c_{11} & c_{13} & 0 \\ c_{13} & c_{33} & 0 \\ 0 & 0 & c_{55} \end{bmatrix} \begin{Bmatrix} \varepsilon_{xx} \\ \varepsilon_{xx} \\ \gamma_{xz} \end{Bmatrix} \tag{4}$$

or

$$\{\sigma\} = [c(z)]\{\varepsilon\}.$$

The variation of Young's modulus E in the thickness direction is given by a polynomial in z, e.g.,

$$E(z) = E_0\left(a_1\left(\frac{z}{h}\right)^4 + a_2\left(\frac{z}{h}\right)^3 + a_3\left(\frac{z}{h}\right)^2 + a_4\left(\frac{z}{h}\right) + 1\right), \tag{5}$$

where E_0 is the Young's modulus at $z=0$ and a_1, a_2, a_3 and a_4 are material constants. We assumed that thickness in y direction is large and plain strain assumption can be used. The elasticity matrix $[\boldsymbol{C}]$ is related to the material constants by

$$C = \frac{E(z)}{(1+v)(1-2v)} \begin{pmatrix} 1-v & v & 0 \\ v & 1-v & 0 \\ 0 & 0 & \dfrac{1-2v}{2} \end{pmatrix}. \tag{6}$$

We assume the solution for displacements as

$$u(x,z) = U(z)\cos\xi x, \qquad w(x,z) = W(z)\sin\xi x. \tag{7}$$

Substituting Eq. (7) into (4), we obtain,

$$\begin{pmatrix} \sigma_{xx} \\ \sigma_{zz} \\ \tau_{xz} \end{pmatrix} = \begin{pmatrix} c_{11} & c_{13} & 0 \\ c_{13} & c_{33} & 0 \\ 0 & 0 & G \end{pmatrix} \begin{pmatrix} -\xi U \sin\xi x \\ W' \sin\xi x \\ U' + \xi W \cos\xi x \end{pmatrix}. \tag{8}$$

A prime ($'$) after a variable denotes differentiation with respect to z. Boundary conditions of the beam at $x=0$ and $x=L$ are $w(0,z)=w(L,z)=0$, and $\sigma_{xx}(0,z)=\sigma_{xx}(L,z)=0$, which corresponds to simple support conditions in the context of beam theory. Eq. (8) can be written as

$$\begin{pmatrix} \sigma_{xx} \\ \sigma_{zz} \end{pmatrix} = \begin{pmatrix} S_x \\ S_z \end{pmatrix} \sin\xi x, \qquad \tau_{xz} = T_z \cos\xi x, \tag{9}$$

where

$$\begin{pmatrix} S_x \\ S_z \end{pmatrix} = \begin{pmatrix} c_{11} & c_{13} \\ c_{13} & c_{33} \end{pmatrix} \begin{pmatrix} -\xi U \\ W' \end{pmatrix}, \qquad T_z = G(U' + \xi W). \tag{10}$$

Substituting for σ_{xx}, σ_{zz}, τ_{xz} from Eq. (8) into equilibrium equation (3), we obtain a set of ordinary differential equations in $U(z)$ and $W(z)$,

$$\xi S_x + T_z' = 0, \qquad S_z' - T_z \xi = 0. \tag{11}$$

In order to solve Eq. (11) we employ the Galerkin method. We assume solutions in the form of polynomials in z as follows:

$$\begin{aligned} U(z) &= c_1\phi_1(z) + c_2\phi_2(z) + c_3\phi_3(z) + c_4\phi_4(z) + c_5\phi_5(z), \\ W(z) &= b_1\phi_1(z) + b_2\phi_2(z) + b_3\phi_3(z) + b_4\phi_4(z) + b_5\phi_5(z), \end{aligned} \tag{12}$$

where ϕ's are basis functions, and b's and c's are coefficients to be determined. For simplicity we choose 1, z, z^2, z^3, z^4 as basis functions. That is,

$$\phi_1(z) = 1, \qquad \phi_2(z) = z, \qquad \phi_3(z) = z^2, \qquad \phi_4(z) = z^3, \qquad \phi_5(z) = z^4. \tag{13}$$

Substituting the approximate solution in the governing differential equations, we obtain the residuals. The residuals are minimized by equating their weighted averages to zero,

$$\begin{aligned} &\int_0^h \left(\xi S_x + T_z'\right)\phi_i(z)\,\mathrm{d}z = 0, \quad i = 1, 5, \\ &\int_0^h \left(S_z' - T_z\xi\right)\phi_i(z)\,\mathrm{d}z = 0, \quad i = 1, 5. \end{aligned} \tag{14}$$

Using integration by parts we can rewrite Eq. (14) as

$$\begin{aligned} &\int_0^h \phi_i \xi S_x\,\mathrm{d}z + T_z(h)\phi_i(h) - T_z(0)\phi_i(0) - \int_0^h T_z\phi_i'\,\mathrm{d}z = 0, \\ &\int_0^h S_z\phi_i'\,\mathrm{d}z + \int_0^h T_z\xi\phi_i\,\mathrm{d}z - (S_z(h)\phi_i(h) - S_z(0)\phi_i(0)) = 0, \quad i = 1, 5. \end{aligned} \tag{15}$$

Substituting for $S_x(z)$, $S_z(z)$ and $T_z(z)$ from Eq. (10) into (15) and using the approximate solution for $U(z)$ and $W(z)$ in (12) we obtain

$$\begin{pmatrix} K_{ij}^{(1)} & K_{ij}^{(2)} \\ K_{ij}^{(3)} & K_{ij}^{(4)} \end{pmatrix} \begin{pmatrix} b \\ c \end{pmatrix} = \begin{pmatrix} f_i^{(1)} \\ f_i^{(2)} \end{pmatrix} \tag{16}$$

or

$$[K]\begin{pmatrix} b \\ c \end{pmatrix} = \begin{pmatrix} f_i^{(1)} \\ f_i^{(2)} \end{pmatrix},$$

where

$$\begin{aligned} &K_{ij}^{(1)} = \xi\int_0^h c_{13}\phi_i\phi_j'\,\mathrm{d}z - \xi\int_0^h G\phi_i'\phi_j\,\mathrm{d}z, \quad K_{ij}^{(2)} = -\int_0^h G\phi_i'\phi_j'\,\mathrm{d}z - \xi^2\int_0^h c_{11}\phi_i\phi_j\,\mathrm{d}z, \\ &K_{ij}^{(3)} = -\xi^2\int_0^h G\phi_i\phi_j\,\mathrm{d}z - \int_0^h c_{33}\phi_i'\phi_j'\,\mathrm{d}z \quad K_{ij}^{(4)} = \xi\int_0^h c_{13}\phi_i'\phi_j\,\mathrm{d}z - \xi\int_0^h G\phi_i\phi_j'\,\mathrm{d}z, \qquad i = 1, 5, \\ &f_i^{(1)} = \phi_i(0)T_z(0) - \phi_i(h)T_z(h), \qquad f_i^{(2)} = \phi_i(0)S_z(0) - \phi_i(h)S_z(h), \\ &\begin{pmatrix} b \\ c \end{pmatrix}^{\mathrm{T}} = (\,b_1 \quad b_2 \quad b_3 \quad b_4 \quad b_5 \quad c_1 \quad c_2 \quad c_3 \quad c_4 \quad c_5\,). \end{aligned} \tag{17}$$

Let U_2, W_2, U_3 and W_3 be the displacements at top and bottom surface of top half of the element (top half of the core). Evaluating the expressions for $U(z)$ and $W(z)$ at the top and bottom surfaces and equating them to the surface displacements results in the expression:

$$\begin{pmatrix} U_2 \\ W_2 \\ U_3 \\ W_3 \end{pmatrix} = \begin{pmatrix} 0 & 0 & 0 & 0 & 0 & 1 & h & h^2 & h^3 & h^4 \\ 1 & h & h^2 & h^3 & h^4 & 0 & 0 & 0 & 0 & 0 \\ 0 & 0 & 0 & 0 & 0 & 1 & 0 & 0 & 0 & 0 \\ 1 & 0 & 0 & 0 & 0 & 0 & 0 & 0 & 0 & 0 \end{pmatrix} \begin{pmatrix} b \\ c \end{pmatrix}. \tag{18}$$

This can be compactly expressed as

$$\begin{pmatrix} U_2 \\ W_2 \\ U_3 \\ W_3 \end{pmatrix} = [A] \begin{pmatrix} b_1 \\ \cdots \\ \cdots \\ c_5 \end{pmatrix}. \tag{19}$$

The tractions T_2, P_2, T_3 and P_3 acting on the surface can be related to the functions f_i as follows:

$$\begin{pmatrix} f_1^{(1)} \\ f_2^{(1)} \\ f_3^{(1)} \\ f_4^{(1)} \\ f_5^{(1)} \\ f_1^{(2)} \\ f_2^{(2)} \\ f_3^{(2)} \\ f_4^{(2)} \\ f_5^{(2)} \end{pmatrix} = \begin{bmatrix} -\phi_1(h) & 0 & \phi_1(0) & 0 \\ -\phi_2(h) & 0 & \phi_2(0) & 0 \\ -\phi_3(h) & 0 & \phi_3(0) & 0 \\ -\phi_4(h) & 0 & \phi_4(0) & 0 \\ -\phi_5(h) & 0 & \phi_5(0) & 0 \\ 0 & -\phi_1(h) & 0 & \phi_1(0) \\ 0 & -\phi_2(h) & 0 & \phi_2(0) \\ 0 & -\phi_3(h) & 0 & \phi_3(0) \\ 0 & -\phi_4(h) & 0 & \phi_4(0) \\ 0 & -\phi_5(h) & 0 & \phi_5(0) \end{bmatrix} \begin{pmatrix} T_2 \\ S_2 \\ T_3 \\ S_3 \end{pmatrix} \tag{20}$$

or

$$\begin{pmatrix} f_1^{(1)} \\ \cdots \\ \cdots \\ f_5^{(2)} \end{pmatrix} = [B] \begin{pmatrix} T_2 \\ S_2 \\ T_3 \\ S_3 \end{pmatrix}. \tag{21}$$

From (16), (19) and (21) we obtain:

$$\begin{pmatrix} U_2 \\ W_2 \\ U_3 \\ W_3 \end{pmatrix} = [A][K]^{-1}[B] \begin{pmatrix} T_1 \\ S_1 \\ T_2 \\ S_2 \end{pmatrix} = [K^*] \begin{pmatrix} T_1 \\ S_1 \\ T_2 \\ S_2 \end{pmatrix}.$$

Finally, the stiffness matrix of the top half of the FGM core $[S^{(2)}]$ that relates the surface tractions to the surface displacements is obtained as

$$\begin{pmatrix} T_1 \\ S_1 \\ T_2 \\ S_2 \end{pmatrix} = [K^*]^{-1} \begin{pmatrix} U_2 \\ W_2 \\ U_3 \\ W_3 \end{pmatrix} = [S^{(2)}] \begin{pmatrix} U_2 \\ W_2 \\ U_3 \\ W_3 \end{pmatrix}. \tag{22}$$

In order to satisfy equilibrium, the contributions of the different tractions at each interface should sum to zero. Enforcing the balance and the compatibility of force and displacements at the interfaces enables us to assemble the stiffness matrices of the four elements to obtain a global stiffness matrix S:

$$[S][\,U_1 \quad W_1 \quad U_2 \quad W_2 \quad U_3 \quad W_3 \quad U_4 \quad W_4 \quad U_5 \quad W_5\,]^{\mathrm{T}} = [\,0 \quad p_{\mathrm{a}} \quad 0 \quad 0 \quad 0 \quad 0 \quad 0 \quad 0 \quad 0 \quad 0\,]^{\mathrm{T}}. \tag{23}$$

The displacements $U_1, W_1, \ldots, W_5$, are obtained by solving Eq. (23). The displacement field along with the constitutive relations is used to obtain the stress field in each element.

2. Contact problem

Contact problems for finite thickness layers can be solved using numerical methods. Sankar and Sun (1983) used two types of numerical methods, point matching technique and assumed stress distribution method. The point matching method is essentially a numerical technique to solve the integral equations of the contact problem. However, this method fails when the contact area is too small because of numerical difficulties. In the assumed contact stress distribution method, the contact stresses are assumed to be of Hertzian form, i.e., similar to that of contact of a half-plane. The contact stresses take the shape of a semi-ellipse. A contact length is assumed and the contact stresses are expressed in terms of only one unknown, the peak contact stress. Requiring that the deflections beneath the contact region match the indentor profile one can solve for the peak contact stress.

The dimensions of the sandwich beam used in the present study are shown in Fig. 3. The length of the beam is L, the core thickness is $2h$ and the face sheet thickness is h_{f}. The contact length $2c$, was considered as known and the response quantities (stresses, deflection) were calculated for a given contact length. Indentation, α is defined as the difference in the vertical displacements of the indenter and the corresponding point on the bottom side of the beam.

The stress distribution under the indenter (Fig. 4) is assumed to be of the semi-elliptical form:

$$p(x) = p_{\max}\sqrt{1 - \frac{x^2}{c^2}}, \tag{24}$$

where $p_{\max}$ is maximum value of the stress at center (unknown).

We assume a similar stress distribution with some arbitrary $p_{\max}$, say p_M, and compute the vertical displacements of the points in the contact zone using the method described in the previous section. Writing $p(x)$ in the form of a Fourier sine series we obtain

$$p(x) = \sum_{n=1,3,\ldots}^{\infty} p_n \sin\frac{n\pi x}{L}, \tag{25}$$

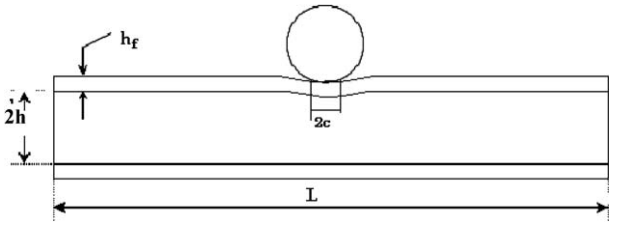

Fig. 3. Dimensions of the sandwich panel and the contact length $2c$.

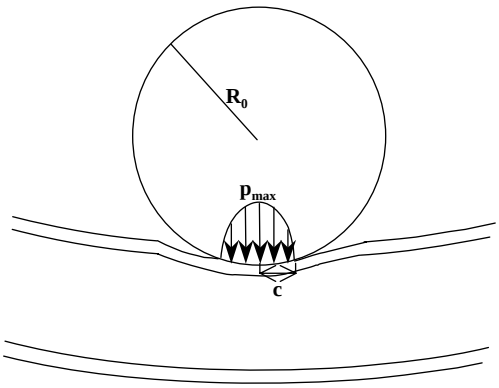

Fig. 4. The stress distribution under the indenter.

where

$$p_n = \frac{2p_M}{n} \sin\left(\frac{n\pi}{2}\right) J_1\left(\frac{n\pi c}{L}\right), \tag{26}$$

and J_1 is the Bessel function of first order. Using the method developed in the previous section one can find the vertical displacements of the points in the contact zone. From geometrical considerations, for contact lengths smaller in comparison with the radius of indenter, we use the following approximate relation:

$$\delta(x) = w(x) - w(x_0) = \frac{x^2}{2R'(x)}, \tag{27}$$

where $w(x_0)$ is vertical displacement at the middle point (see Fig. 5). In (27) R' is the radius of curvature at x. It is found that R' is almost constant (usually, more then 70% of R' distribution lies within one standard deviation of the mean value). Then the average radius of curvature of the deformed top face sheet can be derived as

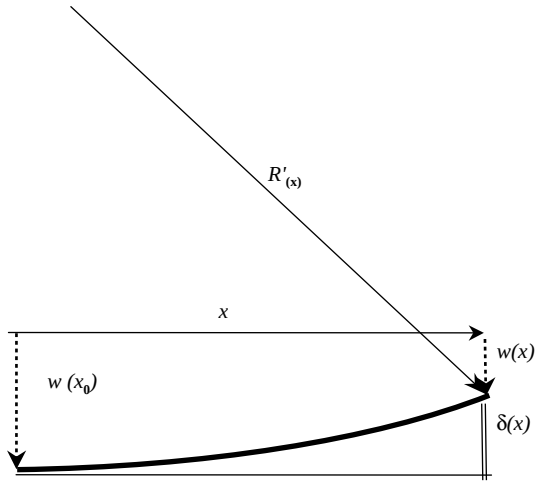

Fig. 5. Illustration of relation between w deflection and radius of curvature of the deformed surface.

$$R = \frac{1}{c}\int_0^c R'(x)\,\mathrm{d}x. \tag{28}$$

Generally R is different from the radius of the intender R_0. But, the displacements vary linearly with the load and hence the peak stress $p_{\max}$ required producing a radius R_0 is given by

$$p_{\max} = p_M \frac{R}{R_0}. \tag{29}$$

Once $p_{\max}$ is known, vertical displacements and the indentation can be calculated. Plots for several examples are presented and discussed in Section 4.

3. Impact problem

After we solve the static contact problem we apply the methods to the problem of low-velocity impact of functionally graded sandwich panels. Solving the static contact problem first and combining the solution with the dynamic response of the sandwich panel obtained via simple spring-mass models (quasi-static assumption) accomplish this. The use of static load-deflection behavior of the sandwich beam in the impact analysis needs some justification. In general the wave propagation effects, especially through the thickness of the core, should be considered in impact response of sandwich panels. This will be crucial when spalling type damage occurs in the panels. However, a study by Sankar (1992) showed that for very large impactor mass compared to that of the target plate and for very low impact velocities compared to the wave velocity in the target medium, quasi-static assumptions yield sufficiently accurate results for impact force history and ensuing stresses in the impacted plate.

The sandwich beam is modeled as a combination of two springs (Shivakumar et al., 1985), a linear spring to account for the global deflection and a nonlinear spring to represent the local indentation effects as depicted in Fig. 6.

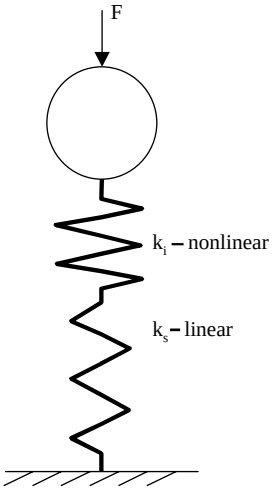

Fig. 6. Low-velocity impact model.

Using the numerical results from the contact problem we determined spring constants k_i and k_s and the exponent n such that

$$F = k_i \alpha^n, \tag{30}$$

$$F = k_s w_b, \tag{31}$$

where F is the total load, α is the core indentation, w_b is the vertical displacement of the core at the at bottom face sheet interface.

The displacement of the impactor is calculated as the sum of indentation depth (core compression) and the global deflection of the sandwich beam:

$$w = \alpha + w_b = \frac{F}{k_s} + \left(\frac{F}{k_i}\right)^{1/n}. \tag{32}$$

The work done by the impactor during the impact event can be expressed as

$$W = \int_0^w F\,\mathrm{d}w = Fw - \int_0^F w\,\mathrm{d}F = Fw - \int_0^F \left(\frac{F}{k_s} + \left(\frac{F}{k_i}\right)^{1/n}\right)\mathrm{d}F = \frac{F^2}{2k_s} + \frac{1}{n+1}\frac{F^{1+1/n}}{2k_i^{1/n}}. \tag{33}$$

Considering that the impactor kinetic energy is equal to the work done or the strain energy stored in the springs, the maximum contact force can be calculated from

$$\frac{F_{\max}^2}{2k_s} + \frac{F_{\max}^{1+1/n}}{(n+1)k_i^{1/n}} = \frac{1}{2}mv_0^2, \tag{34}$$

where m and v_0 are, respectively, the mass and impact velocity of the impactor.

We used the results of the static contact problem to determine the constants that described the stiffness and compression of FG sandwich beam. Using these material properties and the quasi-static model we solved for maximum contact force in the case of low-velocity impact of FG sandwich beam. Using this maximum value, we determined and compared the maximum normal and shear strains in the core. Results for several examples are presented in the next section.

4. Results and discussions

A sandwich beam, with length $L = 0.2$ m, core thickness $h = 20 \times 10^{-3}$ m and facesheet thickness $h_f = 0.3 \times 10^{-3}$ m is considered to investigate the effects of varying core properties through the thickness. The face-sheet Young's modulus was chosen as 50 GPa.

Although this method can be applied to a general form of E as in Eq. (5), in the present paper, for core Young's modulus, we consider two cases (Fig. 7): linear symmetric about midplane and linear asymmetric. The variation of E with respect to z for the two cases is given below and in Fig. 6:

$$E^{\mathrm{sym}} = E_0^{\mathrm{sym}}\left(\frac{E_h^{\mathrm{sym}} - E_0^{\mathrm{sym}}}{E_0^{\mathrm{sym}}}\frac{|z|}{h} + 1\right) \quad \text{if } z \in [-h, h], \tag{35}$$

$$E^{\mathrm{asym}} = E_0^{\mathrm{asym}}\left(\frac{E_h^{\mathrm{asym}} - E_0^{\mathrm{asym}}}{2E_0^{\mathrm{asym}}}\frac{z}{h} + \frac{E_0^{\mathrm{asym}} + E_h^{\mathrm{asym}}}{2E_0^{\mathrm{asym}}}\right) \quad \text{if } z \in [-h, h], \tag{36}$$

where $2h$ is the core thickness; E_0^{sym} is the Young's modulus at the midplane for symmetric case; E_0^{asym} is the Young's modulus at the bottom surface for asymmetric case. E_h^{sym} is the sandwich core Young's modulus at face sheet interfaces for symmetric case; E_h^{asym} is the sandwich core Young's modulus at top face sheet interface for asymmetric case. Three different variations such that $E_h = E_0 \times (1, 5, 10)$ are considered. E_h is the

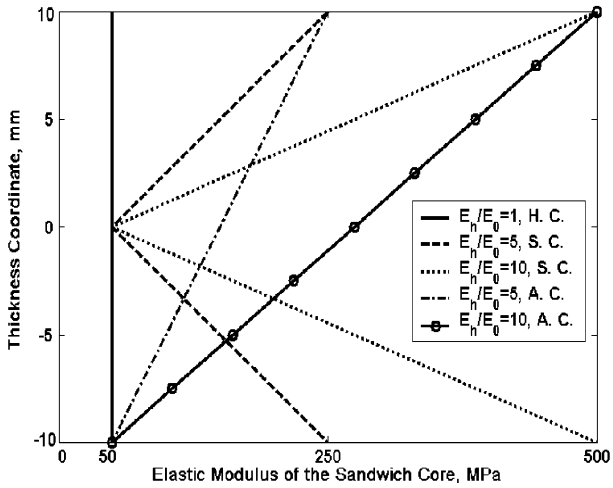

Fig. 7. Through the thickness variations of core modulus considered for the functionally graded sandwich beam. (H.C.: homogeneous core; S.C.: symmetric core; A.C.: asymmetric core.)

core modulus at face sheet interfaces for symmetric case and is the sandwich core modulus at top face sheet interfaces for asymmetric case.

Poisson's ratios are $v = 0.35$ for the core and $v_f = 0.25$ for the face-sheet material. The intender is a cylinder with a radius of 10×10^{-3} m. The width of the cylinder and the width of the sandwich panel in y-direction are assumed to be unity. The cylinder is made of steel and its mass is $m = 15.7$ kg. The impact velocity of the impactor is $v_0 = 6$ m/s and the kinetic energy is $K = 282.2$ J.

Fig. 8 depicts the contact load-indentation (beam thickness compression) relations for various beams. It may be noted that the contact stiffness is higher when the core density is also higher near the face sheet. For an indentation of 0.2 mm the contact force increases by a factor of about 8 when the core modulus at the

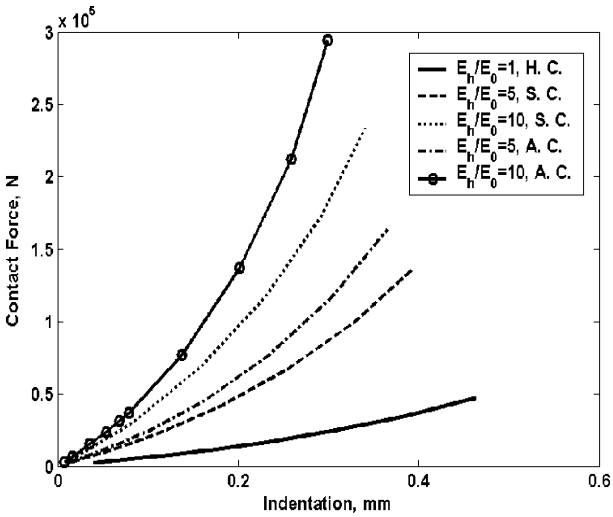

Fig. 8. Variation of contact force with indentation depth in functionally graded beams. (H.C.: homogeneous core; S.C.: symmetric core; A.C.: asymmetric core.)

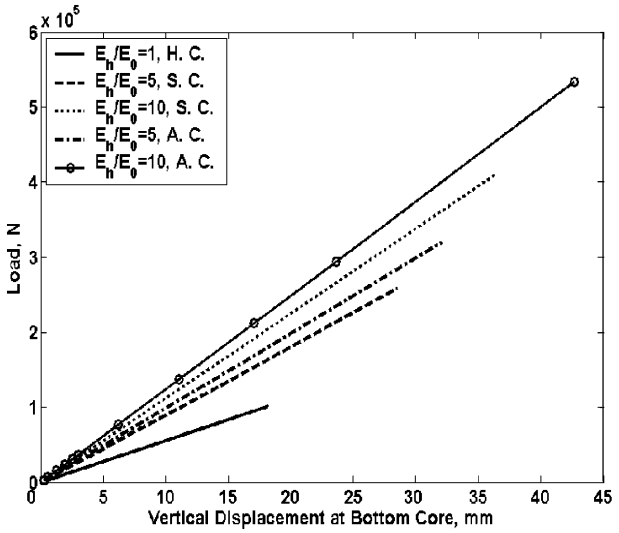

Fig. 9. Relation between contact force and the vertical displacement at bottom midpoint in functionally graded sandwich beams. (H.C.: homogeneous core; S.C.: symmetric core; A.C.: asymmetric core.)

interface increases by a factor of 10. Of course, there is a shielding effect due to the stiff face sheet and that is why the increase in contact force is not in the same order as the core stiffness. The load-indentation relations are needed in solving the problem of low-velocity impact of a rigid impactor and the sandwich beam.

The central deflection of the beam as a function of applied force is plotted in Fig. 9. The relations are approximately linear. The FG core affects the stiffness of the beam as the high-density core near the face sheet contributes significantly to the flexural stiffness of the beam. Also, it can be noted that the asymmetric beam is stiffer than the symmetric one because near the top face sheet (where the contact occurs) the Young's modulus for the asymmetric case is larger than that for symmetric case. Using these results we determined the contact stiffness that describe the relation between the contact force and indentation (31) and the global stiffness that relates the contact force to the vertical displacement (32). These constants are needed for the quasi-static model. The total loads and maximum vertical displacements for various contact lengths are presented in Fig. 9 in order to present the trend. Although the range of deflection in Fig. 9 are much larger (~40 mm) for small deflection theory, the impactor mass and velocity in the example impact problems are such that the maximum deflection (~8 mm) does not exceed the limits for linear elastic approach.

In order to determine if the core can withstand the contact loads due to impact we need to compute not only the maximum stresses in the core but also need to compare them with corresponding strength values. Since the strength of a FG core is expected to vary with location and also we do not have sufficient data on strength, it was decided to calculate the maximum strains. We assume that the maximum strain theory will hold well at all densities and thus strains can be used to determine the efficacy of FG cores compared to uniform cores. The variation of maximum normal strain ε_{xx} and maximum shear strain γ_{xz} in the core for a given contact force are plotted in the Figs. 10 and 11, respectively. Using the maximum contact force values for a given impact energy (282 J) in various panels we determined the maximum strains for that impact event. These results are summarized in Table 1.

From Table 1 one can notice that maximum normal strain corresponding to the maximum impact load decreases by approximately 40% as the Young's modulus of material at the top of the core increases by a factor of 10 for symmetric case, and by approximately 35% for the asymmetric cases. Also the maximum

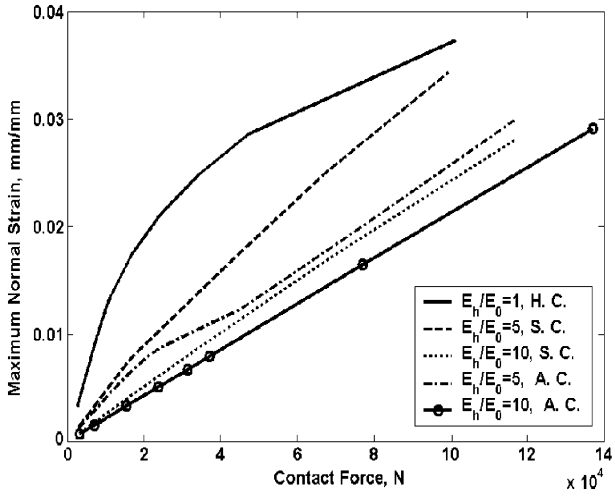

Fig. 10. Contact force vs. maximum normal strain for beams with FGM core and homogeneous core. (H.C.: homogeneous core; S.C.: symmetric core; A.S.: asymmetric core.)

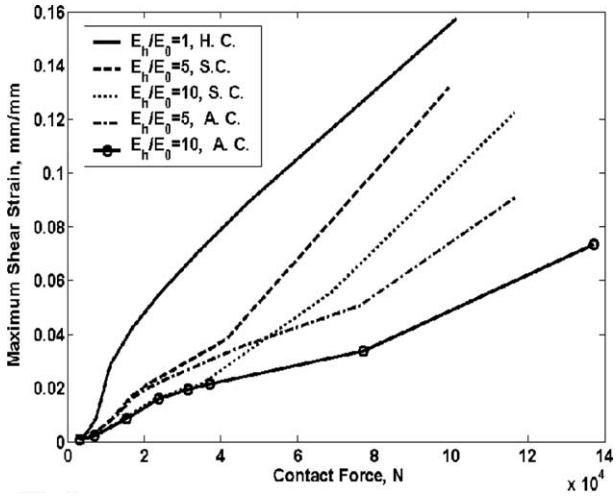

Fig. 11. Contact force vs. maximum shear strain for beams with FGM core and homogeneous core. (H.C.: homogeneous core; S.C.: symmetric core; A.C.: asymmetric core.)

shear strain corresponding to the maximum impact load decreases by approximately 60% as the Young's modulus of the asymmetric material at top of the core is increased by a factor of 10. For the symmetric core case the reduction is with approximately 30% when Young's modulus of the symmetric material at top of the core is increased by a factor of 10. An interesting conclusion is that the maximum strain corresponding to the maximum impact load for asymmetric core is smaller than maximum strain for symmetric core. The reason for this is that the asymmetric core is stiffer in a larger region in the vicinity of contact compared to the symmetric core.

From Fig. 9, one can notice that the FG core affects the stiffness of the beam as the high-density core near the face sheet contributes significantly to the flexural stiffness of the beam. Hence, to maintain the

Table 1
Maximum normal and shear strains for a given impact energy of 282 J

Core type	E_h/E_0	F_{max} (N)	ε_x		γ_{xz}	
			Maximum	% Change	Maximum	% Change
Uniform	1	5.45×10^4	0.0300	–	0.0978	–
FG, symmetric	5	7.03×10^4	0.0257	14.3	0.0830	15.1
FG, symmetric	10	7.89×10^4	0.0194	35.3	0.0700	28.4
FG, asymmetric	5	7.39×10^4	0.0195	35.0	0.0500	48.9
FG, asymmetric	10	8.31×10^4	0.0176	41.3	0.0368	62.3

FG denotes functionally graded core.
The % change in strain in FG cores is with respect to the maximum strain in uniform core.

same flexural stiffness for different core materials, the core thickness is varied as described below. The flexural stiffness is defined as

$$D_{ij} = \int_{-\left(\frac{h}{2}+h_f\right)}^{\frac{h}{2}+h_f} C_{ij} z^2 \, dz, \tag{37}$$

where C_{ij} are stiffness coefficients of the constituents, face sheets and the core, h is the core thickness and h_f is the face sheets thickness. The core thicknesses of the FG cores were chosen such that the flexural stiffness of the sandwich beam will be equal to that of the beam with homogeneous core. That is

$$D_{11}^{FG} = D_{11}^{hom}. \tag{38}$$

The results for core thickness obtained using this method are presented in Table 2. All the thicknesses for FGM obtained in this way are smaller than that for homogeneous core.

The load-deflection behavior of the sandwich beams having the same flexural stiffness is presented in Fig. 12 and in Table 2. The results indicate that the beam stiffness is not the same for all beams since we have not considered shear deformation effects in Eq. (38).

Since the beam stiffness include both flexural and shear stiffness, an approximate method was used to obtain the thicknesses of FGM cores such that these beams exhibit the same stiffness as the homogenous core beam: the thicknesses of FGM were chosen such that the slopes of load-deflection curves to be the same as the slope of load-deflection curve for the homogeneous core. The results are presented in Table 2. One can notice that the values for the core thicknesses in the case of same global stiffness are slightly larger than those for the case of same flexural stiffness.

The impact analysis was repeated for the two sets of beams: having the same flexural stiffness and having the same total stiffness, and the results for maximum normal and shear strains in the core for all cases, for a given impact energy are presented in Figs. 13 and 14. From those plots some important results can be

Table 2
Core thicknesses for different materials with same flexural stiffness D_{11} and same global stiffness

Core type	E_h/E_0	For constant D_{11}		For constant global stiffness	
		Core thickness, h (mm)	Global stiffness, k_s (MN/m)	Core thickness, h (mm)	Global stiffness, k_s (MN/m)
Uniform	1	20	5.5	20	5.65
Symmetric	5	12.58	4.4	14.44	5.65
Symmetric	10	10.08	3.67	12.88	5.65
Asymmetric	5	13.82	5.5	13.82	5.65
Asymmetric	10	11.28	4.78	12.32	5.65

H.C.: homogeneous core; S.C.: symmetric core, A.S.: asymmetric core.

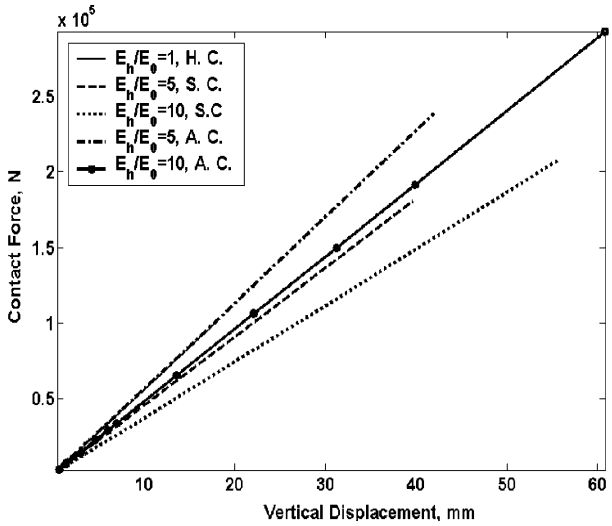

Fig. 12. Variation of contact force with global deflection at bottom midpoint in functionally graded beams with different core thickness but the same flexural stiffness D_{11}. (H.C.: homogeneous core; S.C.: symmetric core; A.S.: symmetric core.)

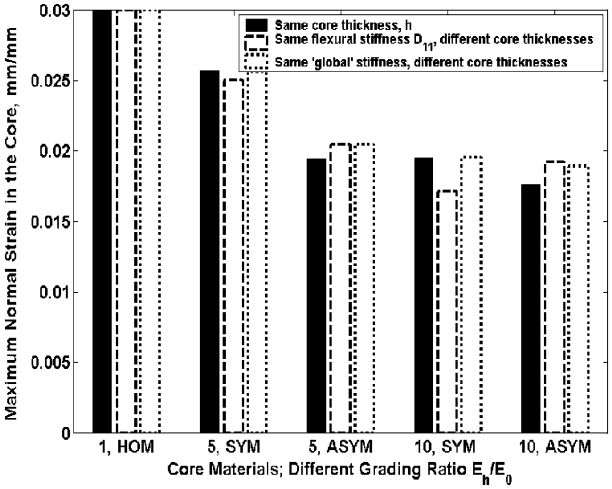

Fig. 13. Comparison of maximum normal strains for different core materials. $E_h/E_0 = 1$ represents the homogeneous core.

inferred. For both symmetric and asymmetric material as the ratio E_h/E_0 increases the material become stiffer and the maximum strains decrease. Also the maximum strains corresponding to the maximum impact load for asymmetric core are smaller than maximum strains for symmetric core as the asymmetric core material is stiffer in the region of contact. For the same material (symmetric or asymmetric, with same ratio E_h/E_0) as the core thickness decreases, the total stiffness also decreases and the maximum shear strain corresponding to the maximum impact load increases. Overall the "most graded" (with the largest ratio E_h/E_0) asymmetric core gives the smaller maximum strains. As a final conclusion, the results indicate that functionally graded cores can be used effectively to mitigate or completely prevent impact damage in sandwich composites.

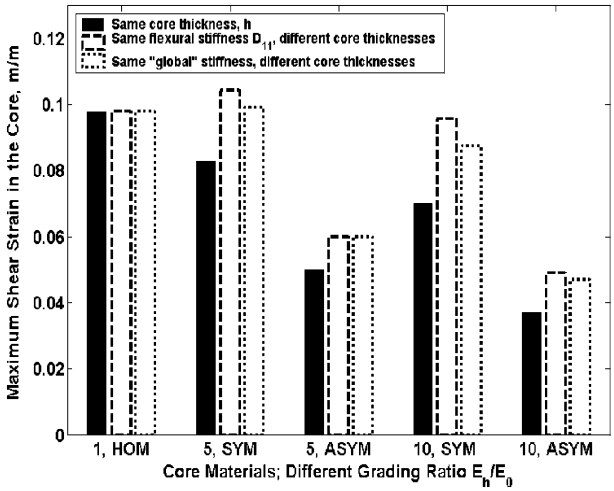

Fig. 14. Comparison of maximum shear strains for different core materials. $E_h/E_0 = 1$ represents the homogeneous core.

Acknowledgments

This research was supported by the NASA Langley Research Center Grant NAG-1-1887 to University of Florida. Support of the NASA CUIP (URETI) Grant NCC3-994 managed by Claudia Mayer at Glenn Research Center is also acknowledged.

References

Abid Mian, M., Spencer, A.J.M., 1998. Exact solutions for functionally graded and laminated elastic materials. Journal of the Mechanics and Physics of Solids 46 (12), 2283–2295.

Aboudi, J., Pindera, M-J., 1995. Thermoelastic theory for the response of materials functionally graded in two directions with applications to the free-edge problem. NASA TM 106882, Lewis Research Center, Cleveland, OH.

Aboudi, J., Arnold, S.M., Pindera, M-J., 1994a. Response of functionally graded composites to thermal gradients. Composites Engineering 4, 1–18.

Aboudi, J., Pindera, M.-J., Arnold, S.M., 1994b. Elastic response of metal matrix composites with tailored microstructures to thermal gradients. International Journal of Solids Structures 31, 1393–1428.

Aboudi, J., Pindera, M.J., Arnold, S.M., 1995. Thermo-inelastic response of functionally graded composites. International Journal of Solids Structures 32 (12), 1675–1710.

Aboudi, J., Pindera, M.-J., Arnold, S.M., 1999. Higher-order theory for functionally graded materials. Composites Part B 30, 777–832.

Amada, S., Untao, S., 2001. Fracture properties of bamboo. Composites Part B 32, 451–459.

Amada, S., Ichikawa, Y., Munekata, T., Nagase, V., Shimizu, H., 1997. Fiber texture and mechanical graded structure of bamboo. Composites Part B 28, 13–20.

Apetre, N.A., Sankar, B.V., Venkataraman, S., 2002. Indentation of a sandwich beam with functionally graded core. In: Proceedings of the 43rd AIAA Structures, Structural Dynamics and Materials Conference, AIAA Paper 2002-1683, Denver, CO.

Apetre, N.A., Sankar, B.V., Ambur, D.R., 2003. Functionally-graded sandwich core with arbitrary variation in properties. In: Proceedings of the 44th AIAA Structures, Structural Dynamics and Materials Conference, AIAA Paper 2003-1947, Norfolk, VA.

Avery, J.L., Sankar, B.V., 2000. Compressive failure of sandwich beams with debonded facesheets. Journal of Composite Materials 34 (14), 1176–1199.

Delale, F., Erdogan, F., 1983. The crack problem for a nonhomogeneous plane. ASME Journal of Applied Mechanics 50, 609–614.

El-Hadek, M., Tippur, H.V., 2003. Dynamic fracture parameters and constraint effects in functionally graded syntactic epoxy foams. International Journal of Solids Structures 40, 1885–1906.

Fukui, Y., 1991. Fundamental investigation of functionally graded materials manufacturing system using centrifugal force. JSME International Journal Series III 34 (1), 144–148.

Fukui, Y., Yamanaka, N., Enokida, Y., 1997. Bending strength of an AI-AI3Ni functionally graded material. Composites Part B 28, 37–43.

Koizumi, M., 1997. FGM activities in Japan. Composites Part B 28, 1–4.

Lambros, J., Santare, M.H., Li, H., Sapna, G.H., 1999. A novel technique for the fabrication of laboratory scale model of FGM. Experimental Mechanics 39 (3), 184–190.

Marrey, R.V., Sankar, B.V., 1993. Stress gradient effects on stiffness and strength of textile composites. In: Bert, C.W., Birman, V., Hui, D. (Eds.), Composite Materials and Structures AD 37, AMD 179 ASME Winter Annual Meeting. pp. 133–148.

Pindera, M.-J., Dunn, P., 1995. An evaluation of coupled microstructural approach for the analysis of functionally graded composites via the finite element method. NASA CR 195455. Lewis Research Center, Cleveland, OH.

Reddy, J.N., 2000. Analysis of functionally graded plates. International Journal for Numerical Methods in Engineering 47, 663–684.

Reddy, J.N., Cheng, Z.Q., 2001. Three-dimensional thermomechanical deformations of functionally graded rectangular plates. European Journal of Mechanics A/Solids 20, 841–855.

Rooney, F., Ferrari, M., 1999. Tension, bending and flexure of functionally graded cylinders. International Journal of Solids and Structures 38, 413–421.

Sankar, B.V., 1992. Scaling of low-velocity impact for symmetric laminates. Journal of Reinforced Plastics and Composites 11 (3), 296–309.

Sankar, B.V., 2001. An elasticity solution for functionally graded beams. Composites Science and Technology 61, 689–696.

Sankar, B.V., Sun, C.T., 1983. Indentation of a beam by a rigid cylinder. International Journal of Solids and Structures 19, 293–303.

Sankar, B.V., Tzeng, J.T., 2002. Thermal stresses in functionally graded beams. AIAA Journal 40 (6), 1228–1232.

Sarkar, P., Datta, S., Nicholson, P.S., 1997. Functionally graded ceramic/ceramic and metal/ceramic composites by electrophoretic deposition. Composites Part B 28, 49–56.

Shivakumar, K.N., Elber, W., Illg, W., 1985. Prediction of impact force and duration during low-velocity impact on circular composite laminates. Transaction of ASME, Journal of Applied Mechanics 52, 674–680.

Sun, C.T., Sankar, B.V., 1985. Smooth indentation of an initially stressed orthotropic beam. International Journal of Solids Structures 21 (2), 161–176.

Suresh, S., 2001. Graded materials for resistance to contact deformation and damage. Science 292, 2447–2451.

Suresh, S., Mortensen, A., 1998. Fundamentals of Functionally Graded Materials. IOM Communications Limited, London, United Kingdom.

Vel, S.S., Batra, R.C., 2002. Exact solution for thermoelastic deformations of functionally graded thick rectangular plates. AIAA Journal 40 (7), 1421–1433.

Vel, S.S., Batra, R.C., 2003. Three-dimensional analysis of transient thermal stresses in functionally graded plates. International Journal of Solids and Structures 40, 7181–7196.

Vel, S.S., Batra, R.C., 2004. Three-dimensional exact solution for the vibration of functionally graded rectangular plates. Journal of Sound and Vibration 272 (3–5), 703–730.

Venkataraman, S., Sankar, B.V., 2001. Analysis of sandwich beams with functionally graded core. In: Proceedings of the 42nd AIAA Structures, Structural Dynamics and Materials Conference, AIAA Paper 2001-1281. Seattle, WA.

Watari, F., Yokoyama, A., Saso, F., Uo, M., Kawasaki, T., 1997. Fabrication and properties of functionally graded dental implant. Composites Part B 28, 5–11.

Woo, J., Meguid, S.A., 2000. Nonlinear analysis of functionally graded plates and shallow shells. International Journal of Solids and Structures 38, 7409–7421.

Zhu, H., Sankar, B.V., 2004. A combined Fourier series–Galerkin method for the analysis of functionally graded beams. Journal of Applied Mechanics 71 (3), 421–424.